Metrological Investigations on the Stability of Reference Points of VGOS Antennas

C. Eschelbach[1], M. Lösler[1], R. Haas[2]

Abstract The reference points of geodetic infrastructure such as radio telescopes used for Very Long Baseline Interferometry (VLBI) form the global geodetic reference frame. The accuracy and the reliability of the established frame therefore depend on the spatio-temporal stability of the reference points. Usually, the stability of an antenna reference point is evaluated selectively as part of complex local tie measurement campaigns. These measurement campaigns commonly apply Global Navigation Satellite System (GNSS) techniques and conventional terrestrial instruments to obtain the reference point position indirectly with millimeter precision w.r.t. the global frame. However, the corresponding measurement configurations are almost insensitive to detecting the smallest position variations, especially when various effects overlap inseparably. To quantify even the smallest variations, specific measurement concepts and advanced instruments are required. For that purpose, high-precise laser trackers are recommended. The Onsala Space Observatory hosts two modern broadband radio telescopes participating in the VLBI Global Observing System (VGOS), namely the Onsala Twin Telescopes. By applying an innovative measuring concept using a laser tracker together with a plane mirror, we directly measured azimuth-dependent vertical displacements of about 30 µm. Small horizontal deviations of about 300 µm were also detected by the laser tracker measurements, indicating a slightly asymmetrical arrangement of telescope components in the sub-millimeter range.

1. Frankfurt University of Applied Sciences, Laboratory for Industrial Metrology, DE-60318 Frankfurt am Main, Germany
2. Chalmers University of Technology, Onsala Space Observatory, SE-439 92 Onsala, Sweden

Keywords Radio telescope, Reference point, Deformation, Laser tracker, Metrology, VGOS

1 Introduction

Geodetic VLBI is known as one of the key technologies for realizing a precise global geodetic reference system, e.g., in the form of the International Terrestrial Reference Frame (ITRF). The reference points of the space-geodetic techniques such as Satellite Laser Ranging (SLR), Doppler Orbitography and Radiopositioning Integrated by Satellite (DORIS), GNSS, and VLBI form the physical realization of the ITRF. The accuracy and the reliability of such an established frame depend on the spatio-temporal stability of the reference points. Reference points of VLBI radio telescopes are generally determined as part of recurring local tie measurement campaigns that are carried out at regular intervals, typically every 2–3 years [6]. Automated measurement concepts reduce the measurement effort and reference points can be determined monthly, weekly, or even daily [2, 7]. Currently, these measurement concepts are only used by a few stations.

Local tie measurement campaigns usually combine GNSS and conventional terrestrial instruments to obtain the reference points indirectly with millimeter precision w.r.t. the global frame [3, 8, 10]. However, the results depend on the measurement configurations and analysis procedures [1, 9]. Moreover, they are almost insensitive to detecting the smallest variations in the position, especially when various effects overlap inseparably. For that reason, high-precise laser trackers in-

tegrated into specific measurement configurations are predestined to quantify even the smallest variations.

The Onsala Space Observatory is a so-called fundamental geodetic site, which hosts instruments of two different space-geodetic techniques, i.e., GNSS and VLBI. The observatory is both an active network station within the International GNSS Service (IGS) as well as in the International VLBI Service for Geodesy and Astrometry (IVS). In addition to several GNSS antennas, the observatory operates in total four large radio telescopes (Figure 1). One of these is used for astronomy only, one is a shared instrument used for both astronomy and geodetic/astrometric VLBI, and the two modern broadband VGOS radio telescopes—the Onsala Twin Telescopes (OTT)—are used exclusively for geodetic/astrometric VLBI.

Fig. 1 VLBI radio telescopes operated at the Onsala Space Observatory: the 25-m (left) and the radome-enclosed 20-m legacy telescopes, as well as two 13.2-m VGOS antennas.

In this contribution, the stability of the OTT reference points is investigated. In order to directly observe possible vertical and horizontal variations, laser trackers were applied in combination with a plane mirror. The measurement concept is presented in Section 2. Section 3 describes the data preparation. The analysis results are presented and discussed in Section 4. Finally, Section 5 concludes this contribution.

2 Measuring Configuration

Reference points of radio telescopes are usually inaccessible and cannot be observed by direct measurements. For this reason, several auxiliary values are measured and the reference point is determined using an indirect approach. The resulting reference point is therefore comparable to an average of all measurements, where small effects in individual measurements are masked by the large number of overall observations. In the field of outlier detection, this behavior is referred to as the *swamping effect*. Consequently, reference point determination approaches are almost insensitive to detecting smallest variations, especially when various effects overlap inseparably. For investigating a particular behavior, it is advisable to observe it directly.

The OTT reference points are inaccessible, but the azimuth axis is realized by a tapered tube. This tube is hollow and can be used to install a height monitoring system like an invar wire [5]. At the ground level, the tube diameter is about 60 cm and it gradually tapers to 3.5 cm at the top end near the azimuth cabin. The tube is Earth-fixed and realizes the azimuth encoder readings. The tube has a side opening on the ground floor to allow installing equipment. The small end piece at the top of the tube allows placing a spherical 1.5″ corner cube reflector (CCR), see Figure 2.

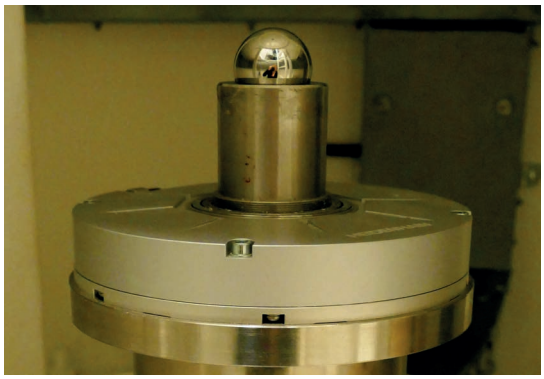

Fig. 2 Spherical 1.5″ corner cube reflector placed on the end piece at the top of the tube close to the azimuth encoder.

We used a laser tracker of type Hexagon AT960 at the ground level to perform measurements to the CCR on the top of the tube. The manufacturer specifies the maximum permissible error of the instrument by 15 mm + 6 µm/m in accordance with ISO 10360-10 [4]. Due to its size, the laser tracker could not be placed inside the tube at ground level to observe the CCR directly. Instead, the laser tracker was placed outside the tube and a small plane mirror was used inside the tube to deflect the AT960 laser beam towards the CCR.

Figure 3 shows the measurement configuration. The laser tracker was located to the west in front of the tube and observed the CCR through the side opening

of the tube via a plane mirror. The tiltable plane mirror was mounted on a cross slide to align the laser beam with the CCR. The tilting axis of the plane mirror pointed to the north.

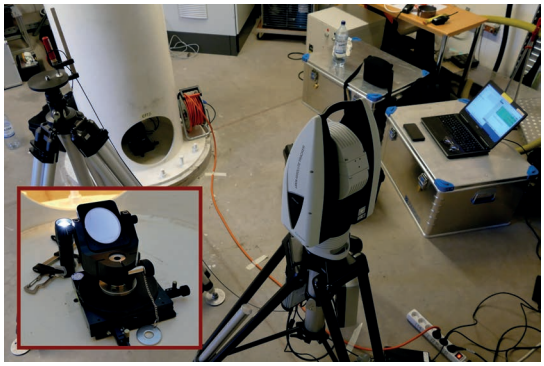

Fig. 3 Laser tracker AT960 in front of the tube observing the CCR via a plane mirror. The plane mirror, mounted on a cross slide, is shown in detail.

Furthermore, a laser tracker Omnitrac II (OT2) manufactured by Automated Precision Inc. (API) was placed inside the telescope azimuth-cabin and oriented to the north. The maximum permissible error of this instrument is specified by 15 mm + 5 µm/m, and again, the spherical 1.5″ corner cube reflector located at the end piece of the tube was observed (Figure 4).

Both configurations were observed at telescope elevations 5°, 45°, and 90°. Each experiment was performed between 0° and 360° in azimuth, using an azimuth step-size of 15°.

In contrast to the first configuration, where both the AT960 laser tracker and the CCR were independent of the telescope rotation and referred to an Earth-fixed frame, the OT2 laser tracker rotated together with the azimuth cabin around the tube. If the tube is assumed to be stable, the OT2 laser tracker therefore measured horizontal displacements of the azimuth cabin, which can be transferred directly to the reference point.

In summary, the motivation to involve these two laser tracker configurations was to separate effects and to perform almost direct measurements. The vertical component was observed by the AT960 laser tracker located on the ground. In addition, the AT960 checked the horizontal stability of the reflector at the end piece of the tube, which connected the OT2 measurements to the Earth-fixed frame.

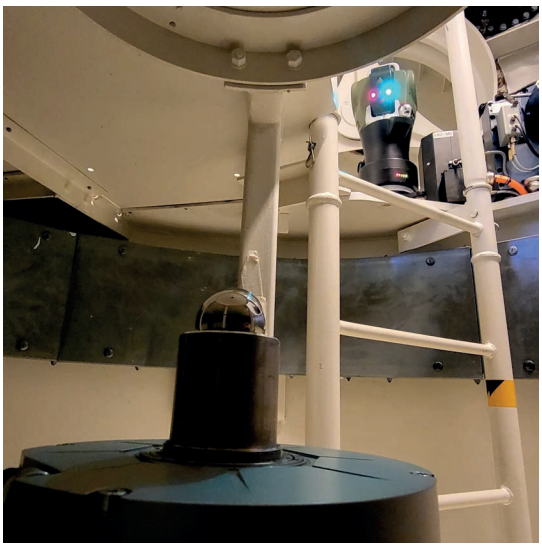

Fig. 4 CCR at the end piece of the tube observed by the OT2 laser tracker located in the azimuth cabin.

3 Data Preparation

As the laser beam of the AT960 laser tracker on the ground is almost parallel to the physical azimuth axis, the vertical displacement,

$$\Delta z_i = s_i - \bar{s}, \tag{1}$$

corresponds directly to the i-th observed slope distance s_i and the average distance denoted by $\bar{s}$.

However, in order to assess the horizontal stability of the tube end from the ground, the polar observations of the AT960 must be converted. Due to the configuration of the planar mirror and the laser tracker, the converted horizontal Cartesian coordinates are readily obtained from

$$x_i = -s_i \sin\left(\zeta_i - \bar{\zeta}\right), \tag{2}$$

$$y_i = -s_i^{\mathrm{H}} \sin\left(\tau_i - \bar{\tau}\right). \tag{3}$$

Here, τ and ζ are the horizontal and vertical angles, respectively, and s_i is the slope distance of the i-th observed position. The horizontal distance is denoted by $s_i^{\mathrm{H}} = s_i \sin\zeta$, and $\bar{\zeta}$ as well as $\bar{\tau}$ are the average angles of ζ and τ, respectively. The relative displacements are

$$\Delta x_i = x_i - \bar{x}, \tag{4}$$

$$\Delta y_i = y_i - \bar{y}, \tag{5}$$

where $\bar{x}$ and $\bar{y}$ denote the average values of x and y, respectively.

Since these displacements are small compared to the height of the radio telescope, Δx and Δy can be approximated by the lengths of circular arcs. Introducing the average angles $\bar{\tau}$ and $\bar{\zeta}$, the relative displacements result from

$$\Delta x_i \approx -s_i \left(\zeta_i - \bar{\zeta}\right), \tag{6}$$

$$\Delta y_i \approx -s_i^{\mathrm{H}} \left(\tau_i - \bar{\tau}\right). \tag{7}$$

Here, $(\tau - \bar{\tau})$ and $\left(\zeta - \bar{\zeta}\right)$ correspond to the central angles of the approximated circle arcs given in radians.

In contrast to the Earth-fixed configuration of the AT960, the OT2 laser tracker was located in the azimuth cabin (Figure 4). Thus, the observed horizontal Cartesian coordinates u and v of the CCR located at the end of the tube refer to a co-rotating cabin-fixed frame. The relative displacements are given by

$$\Delta u_i = u_i - \bar{u}, \tag{8}$$

$$\Delta v_i = v_i - \bar{v}, \tag{9}$$

where $\bar{u}$ and $\bar{v}$ denote the average values of u and v, respectively.

4 Analysis Results

The vertical and horizontal variations are evaluated separately. Whereas the results of the vertical component is presented in Section 4.1, the horizontal changes are discussed in Section 4.2.

4.1 Vertical Variations

The observed height variations of the Onsala Twin Telescopes are depicted as black crosses in Figure 5. Both radio telescopes show an elevation-independent individual pattern and vary slightly within a range of about $\pm 15\,\mu$m.

An adapted cosine function is applied to model and to predict the height variations. This prediction function reads

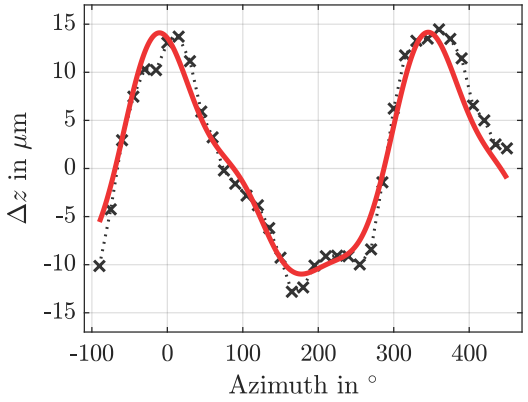

(a) Height variation ONSA13NE

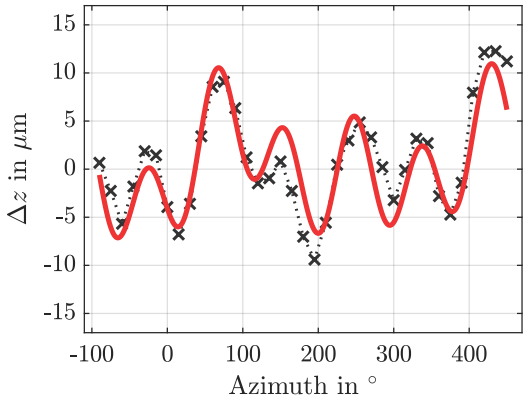

(b) Height variation ONSA13SW

Fig. 5 Height variations of the ONSA13NE (a) and the ONSA13SW (b). Black crosses depict observed values and red curves indicate fitted cosine functions.

$$\Delta \mathrm{z}\,(\alpha) = \frac{a_0}{2} + \sum_{j=1}^{n} a_j \cos\left(2\pi b_j \alpha + c_j\right), \tag{10}$$

where n is the number of dominant series terms, which were initially indicated by the amplitude spectrum of a Fourier series. Equation (10) is known as amplitude-phase form, where a is the amplitude, b corresponds to the frequency, and c denotes the phase. The series coefficients

$$\mathbf{u} = \left[\, a_0 \; a_1 \; \cdots \; a_n \; b_1 \; \cdots \; b_n \; c_1 \; \cdots \; c_n \,\right]^{\mathrm{T}}$$

are obtained by means of least-squares adjustment and summarized in Table 1. The resulting curves are depicted in red in Figure 5.

The height variations are very small but systematic. The observed variations depend on the azimuth angle α but are independent of the elevation angle

Table 1 Estimated coefficients of the amplitude-phase form for ONSA13NE and ONSA13SW.

j	ONSA13NE			ONSA13SW		
	a in µm	b in 1/°	c in °	a in µm	b in 1/°	c in °
0	−1.5	–	–	0.9	–	–
1	11.5	0.16	−6.68	−5.0	0.63	−80.77
2	−2.5	0.32	−142.12	−3.0	0.31	37.16
3	−1.6	0.48	−123.29	−2.9	0.18	62.45

of the radio telescope and are likely due to minor deviations in the telescope structure. However, it is a second-order effect. For comparison, the expansion of the telescope monument due to daily temperature changes has a significantly larger effect on the vertical component. Figure 6 depicts the observed height variations of the ONSA13NE over several days. Changes of about 100 µm can be observed within a single day, even though the radio telescope is equipped with air conditioning.

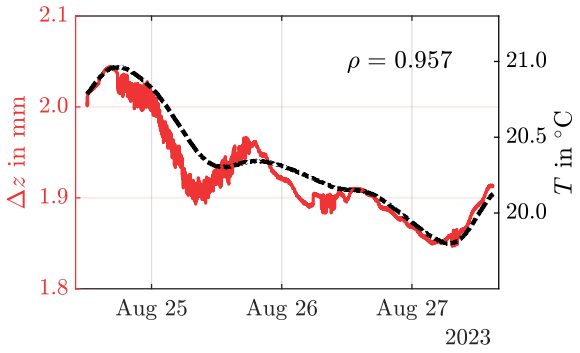

Fig. 6 Multi-day monitoring of the ONSA13NE telescope height using the laser tracker AT960. Height variations are shown in red. Corresponding monument temperature values are plotted in black. The estimated correlation coefficient is $\rho = 0.957$.

Compensating for temperature-induced expansions of the radio telescope is prescribed by the IVS Convention [11]. The correlation between the height variations and the temperature changes shown in Figure 6 is larger than 95 %. For this reason, the OTT are equipped with several PT-1000 sensors to measure the temperature of the structure. In December 2023, invar-based monitoring systems have been installed to directly detect height variations.

4.2 Horizontal Variations

The horizontal variations are investigated in detail exclusively for the ONSA13SW. The three observed series of the OT2 laser tracker located inside the azimuth cabin are shown in Figure 7.

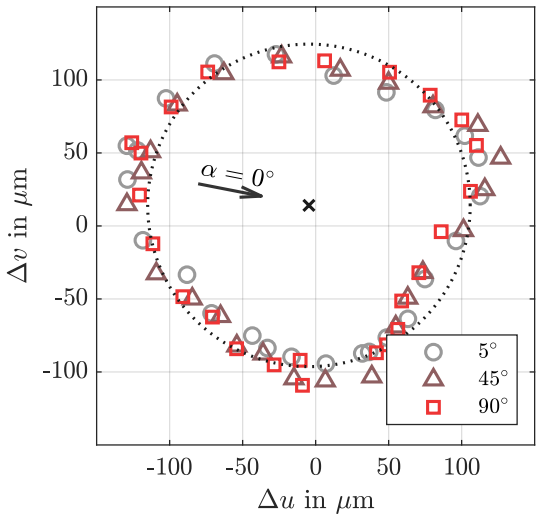

Fig. 7 Horizontal variations w.r.t. the end of the tube observed inside the azimuth cabin using the laser tracker OT2. The grey circle corresponds to the 45° elevation position. The arrow indicates the direction of the first observed position at $\alpha = 0°$. Symbols depicted in different colors relate to different elevation positions under investigation.

The three series are almost identical and the variations are in a range of about ±100 µm. The estimated circle of the 45° elevation position is depicted in grey as a first-order approximation. Since each Earth-fixed position that is not lying on the true rotation axis and is observed in the cabin-fixed frame forms a circle, the radius describes the deviations between the geometric and the physical azimuth axis.

However, as shown in Figure 8, the end of the tube does not provide the expected stable reference. Thus, the circle center depicted by the black cross in Figure 7 does not coincide with the true rotation axis. Variation of about ±300 µm are obtained from the ground measurements using the AT960. Similar to the results depicted in Figure 7, these variations are independent of the elevation position of the radio telescope.

As already mentioned, the tube is part of the Earth-fixed telescope structure and does not rotate in azimuth.

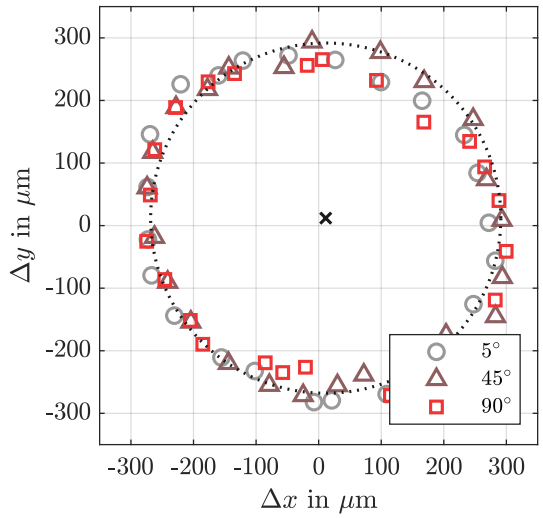

Fig. 8 Horizontal variations of the end of the tube observed from the ground using the laser tracker AT960. The grey circle corresponds to the 45° elevation position. Symbols depicted in different colors relate to different elevation positions under investigation.

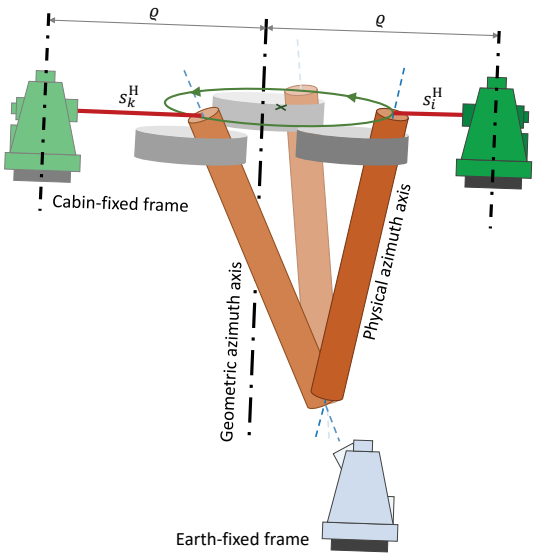

Fig. 9 Schematic representation of the true geometric axis, depicted as dash-dotted black line, and the realized physical axis, depicted as blue dashed line, as well as the measurement configuration w.r.t. the cabin-fixed frame and the Earth-fixed frame. The grey depicted component is asymmetrically arranged and clamps the de-centered tube during the azimuth rotation of the radio telescope.

Thus, the variations observed from the ground result from a forced movement. The tube is clamped by some asymmetrical arranged telescope components.

Figure 9 provides a schematic representation of the wobbling physical axis materialized by the tube and the true geometric axis of rotation. The component depicted in grey is asymmetrically arranged and clamps the decentered tube. The resulting variations forming the green circle are observed by the laser tracker on the ground (Figure 8). Neither the circle center of the resulting green circle nor the end of the tube lie on the true geometric axis. Therefore, the red plotted horizontal distances s_i^H and s_k^H, observed inside the azimuth cabin, vary too. These variations form another circle shown in Figure 7. Again, this circle center does not lie on the true geometric axis.

Using both configurations together, the position of the true geometric azimuth axis can be reconstructed. On the one hand, the circle center observed from the ground relates to the Earth-fixed frame. On the other hand, the radius of the circle measured inside the azimuth cabin corresponds to the deviation between the geometric and the physical azimuth axis. Combining both pieces of information together with the direction of the first observed position shown in Figure 7 yields a point lying on the true geometric azimuth axis.

In summary, the true geometric azimuth axis deviates by about 100 µm from the center of the green circle observed by the instrument on the ground. This rather small value emphasizes the high construction quality of the radio telescope at Onsala. However, the top end of the tube shown in Figure 2 is clamped by slightly asymmetrically arranged components of the telescope. Therefore, it is unsuitable to monitor horizontal variations of the reference point.

5 Conclusion

The reference points of space geodetic techniques are the physical realization of a global geodetic reference system such as the ITRF. The accuracy and the reliability of the established reference frame depend on the spatio-temporal stability of the reference points.

In this contribution, the stability of the reference points of the OTT were investigated. The aim of this investigation was to evaluate pointing-dependent variations of the radio telescopes. For that purpose, an innovative measuring concept involving laser trackers and

a plane mirror was designed. The quantities to be analyzed, i.e., horizontal and vertical variations, should be measured as directly as possible in order to minimize dependencies on, for instance, the geometric configuration or the analysis procedure.

A dependence between the reference point stability and the elevation pointing direction of the radio telescope was not detected. However, some azimuth-dependent effects could be observed. The height of the reference point varies systematically by about $\pm 10\,\mu m$. In comparison to the impact of temperature changes on the monument height, theses variations are second-order effects. A corresponding correction function was derived, which should be applied whenever highest accuracy is aimed for.

Furthermore, small horizontal variations of about $\pm 300\,\mu m$ were detected by the laser tracker measurements. However, these horizontal variations do not coincide with the reference point. A slightly asymmetrical arrangement of telescope components was identified as the reason for the observed variations. The realized physical azimuth axis deviates by about $100\,\mu m$ from the true geometric azimuth axis, which is a small value and emphasizes the high construction quality of the radio telescopes at the Onsala Space Observatory.

Acknowledgements

This research project received funding from the Erna and Victor Hasselblad Foundation (Gothenburg).

References

1. Abbondanza, C., Sarti, P. (2012) Impact of network geometry, observation schemes and telescope structure deformations on local ties: simulations applied to Sardinia Radio Telescope. *Journal of Geodesy*, 86(3), 181–192. doi:10.1007/s00190-011-0507-6
2. Barnéoud, J., Courde, C., Beilin, J., Germerie-Guizouarn, M., Pesce, D., Vidal, M., Collilieux, X., Maurice, N. (2023) Automatic Determination of the SLR Reference Point at Côte d'Azur Multi-Technique Geodetic Observatory. In: *International Association of Geodesy Symposia*, Berlin, Springer. doi:10.1007/1345_2023_223
3. Guillory, J., Truong, D., Wallerand, J.-P., Lösler, M., Eschelbach, C., Mähler, S., Klügel, T. (2023) Determination of the reference point of a radio telescope using a multilateration-based coordinate measurement prototype. *Precision Engineering*, 83, 69–81, 2023. doi:10.1016/j.precisioneng.2023.05.007
4. ISO 10360-10 (2016) *Geometrical product specifications (GPS)*, Acceptance and reverification tests for coordinate measuring systems (CMS) – Part 10: Laser trackers for measuring point-to-point distances. International Organization for Standardization (ISO). `https://www.iso.org/standard/77155.html`
5. Johansson, L.A., Stodne, F., Wolf, S. (1996) The Pisa Project, Variations in the height of the foundation of the 20 meter radio telescope. *Onsala Space Observatory, Chalmers University of Technology*, 178.
6. Klügel, T., Mähler, S., Schade, C. (2012) Ground Survey and Local Ties at the Geodetic Observatory Wettzell. In: U. Schreiber, M. Pearlman, G. Appleby, editors, *Proceedings of the 17th International Workshop on Laser Ranging – Extending the Range*, Frankfurt am Main, Verlag des Bundesamtes für Kartographie und Geodäsie, 48, 127–131.
7. Lösler, M, Haas, R., Eschelbach, C. (2013) Automated and continual determination of radio telescope reference points with sub-mm accuracy: results from a campaign at the Onsala Space Observatory. *Journal of Geodesy*, 87(8), 791–804. doi:10.1007/s00190-013-0647-y
8. Lösler, M, Haas, R., Eschelbach, C. (2016) Terrestrial monitoring of a radio telescope reference point using comprehensive uncertainty budgeting – Investigations during CONT14 at the Onsala Space Observatory. *Journal of Geodesy*, 90(5), 791–804. doi:10.1007/s00190-016-0887-8
9. Lösler, M., Eschelbach, C., Mähler, S., Guillory, J., Truong, D., Wallerand, J.-P. (2023) Operator-software impact in local tie networks: Case study at Geodetic Observatory Wettzell. *Applied Geomatics*, 15, 77–95. doi:10.1007/s12518-022-00477-5
10. Matsumoto, S., Ueshiba, H., Nakakuki, T., Takagi, Y., Hayashi, K., Yutsudo, T., Mori, K., Sato, Y., Kobayashi, T. (2022) An effective approach for accurate estimation of VLBI–GNSS local-tie vectors. *Earth, Planets and Space*, 74(147), 1–14. doi:10.1186/s40623-022-01703-5
11. Nothnagel, A. (2009) Conventions on thermal expansion modelling of radio telescopes for geodetic and astrometric VLBI. *Journal of Geodesy*, 83(8), 787–792. doi:10.1007/s00190-008-0284-z